6-2011

Ion-Beam Analysis of Airborne Pollution

Charles I. Harrington
Union College - Schenectady, NY

ION-BEAM ANALYSIS OF

AIRBORNE POLLUTION

By

Charles Irving Harrington

****

Submitted in partial fulfillment

of the requirements for

Honors in the Department of Physics and Astronomy

UNION COLLEGE

June, 2011

Abstract

HARRINGTON, CHARLES Ion-Beam Analysis of Airborne Pollution. Department of Physics and Astronomy, June 2011.

ADVISOR: DR. MICHAEL VINEYARD

A research program in ion-beam analysis (IBA) of atmospheric aerosols is being developed to study pollution in the Capital District and Adirondack Mountains of New York. The IBA techniques applied in this project include proton induced X-ray emission (PIXE), proton induced gamma-ray emission (PIGE), Rutherford backscattering (RBS), and proton elastic scattering analysis (PESA). These methods are well suited for studying air pollution because they are quick, non-destructive, require little to no sample preparation, and capable of investigating microscopic samples. While PIXE spectrometry is used to analyze most elements from silicon to uranium, the remaining techniques analyze some of the lighter elements to complement PIXE in the study of aerosols. The airborne particulate matter is collected using nine-stage cascade impactors that separate the particles according to size and the samples are bombarded with proton beams from the Union College 1.1-MV Pelletron Accelerator. The reaction products are measured with Si Drift X-ray, Ge gamma-ray, and Si surface barrier charged particle detectors. Here, we report on the progress we have made on the PIGE, RBS, and PESA analysis of aerosol samples.

Contents

1 Introduction

We are developing a research program in ion-beam analysis (IBA) of environmental materials at Union College using the school's particle accelerator to study pollution around New York State. The project will include the study of air, soil, water, fish, and tree samples to help identify the sources and understand the transport, transformation, and effects of the pollutants. Currently, this program is very much in the development stages. In this paper, we report on the progress we made analyzing atmospheric aerosols in Schenectady, NY, during the summers of 2009 and 2010.

Atmospheric aerosols consist of fine particles suspended in air. They are responsible for the haze that lingers in industrial areas and contribute to acid rain. The aerosols may be produced naturally, such as from soil or sea spray, or they may be the product of human processes, like motor vehicles or coal combustion. Fine particle matter less than 2.5 μm ($PM_{2.5}$) poses a threat to human beings because the finer particles have a higher probability of entering the lungs, rather than getting trapped in the nose or throat where they are safely lead to the digestive system. Since airborne pollution can cause damaging health and environmental effects, we study these aerosols to better understand the pollutants and learn how to possibly remove them [1].

Our project compares the composition of the aerosols to the size of their constituent particles. We sampled air from two locations in Schenectady: the Union College boathouse and the Vale cemetery crematorium. At the Union College Ion-Beam Analysis Laboratory (UCIBAL) we studied the aerosol samples using IBA techniques which consisted of proton induced X-ray emission (PIXE), Rutherford backscattering (RBS), proton induced γ-ray emission (PIGE), and proton elastic scattering analysis (PESA). While PIXE is the main focus of the project, we develop the remaining IBA techniques to complement the research.

2 Ion-Beam Analysis Techniques

Ion-beam analysis employs beams of ions, such as helium or hydrogen nuclei, provided by particle accelerators to study the elemental composition and concentration of a material. Particles from the ion-beam, with energies on the order of a few MeV, bombard the target and some fraction of the time collide with its composite atoms. These collisions are picked up by detectors looking for scattered radiation and particles, and we analyze the resulting energy spectra. The four main IBA techniques are proton induced X-ray emission (PIXE), Rutherford backscattering (RBS), proton induced gamma ray emission (PIGE), and proton elastic scattering analysis (PESA). PIXE is the most commonly used IBA technique, as it is capable of detecting the most elements, while the other three techniques work to complement PIXE by focusing on lighter elements.

IBA can be applied to a broad range of topics, including the environmental and biological sciences, as it has a number of advantages over other analytical methods. The techniques consume relatively little time and are versatile. For environmental materials, and particularly aerosols, little to no sample preparation is required. Also, all four techniques can be applied simultaneously, leading to less time consuming experiments. Finally, IBA techniques are non-destructive, meaning samples can be re-run or analyzed by other techniques [1]. In this section, we briefly describe the four main IBA techniques.

2.1 Proton Induced X-Ray Emission (PIXE)

Some fraction of the time, the protons will knock out an inner shell electron of an atom in the target. This causes an outer shell electron to change energy levels and fill the vacancy, emitting an X-ray in the process. With PIXE, we measure the

energies and intensities of these X-rays, which correspond to the elemental make-up and concentration of the target, respectively. PIXE reveals information on most elements from sodium to uranium with good sensitivity as shown in Figure 1. For aerosols, the minimum detection limits of this technique are typically on the order of a few ng/m^3 [1].

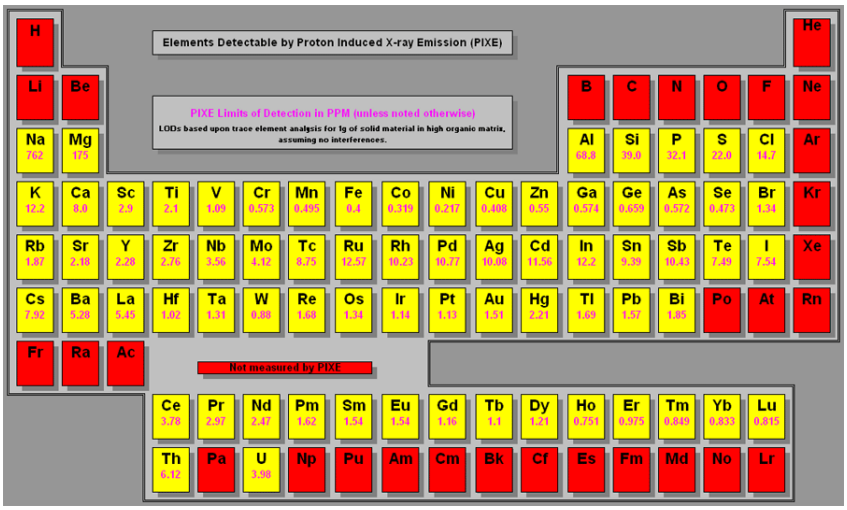

Figure 1: The elements detectable and the minimum detectable limits for PIXE in ppm [2].

2.2 Rutherford Backscattering (RBS)

Whereas PIXE depends on emitted X-rays, RBS looks at scattered particles. As the name of the technique suggests, these particles are the backscattered ions resulting from collisions between the ion-beam and target nuclei. Similar to the other IBA techniques, the energy of the scattered ions determines the elemental composition of the target, and the number of ions determines the mass concentration. RBS has been applied to aerosol samples to find concentrations of carbon, nitrogen, and oxygen with typical minimum detection limits of 2-12 $\mu g/cm^2$ in areal density on sample filters [3].

2.3 Proton Induced Gamma Ray Emission (PIGE)

PIGE is similar to PIXE except this technique depends on γ-ray detection rather than X-ray detection. The γ-ray comes from a nuclear transition where the proton beam collides with the nucleons of an atomic nucleus, subsequently emitting a γ-ray. Since this process is less probable than an electron transition, PIGE is less sensitive than PIXE. For aerosols, PIGE has been used to measure concentrations of sodium and fluorine with minimum detectable limits of around 100 ng/m^3 [3].

2.4 Proton Elastic Scattering Analysis (PESA)

The PESA technique is similar to RBS except that forward scattered ions are measured rather than backscattered ions. The forward scattered ions mostly come from proton collisions with light elements in the target, and so PESA gives information on elements like hydrogen and carbon. This technique is one of the few ways to accurately and non-destructively measure the amount of hydrogen present in a sample, and has been used to measure the hydrogen concentration in aerosol filters. But, this measurement had lower sensitivity than PIXE or PIGE due to large backgrounds under the hydrogen peaks which depend on sample thickness [3].

3 Experimental Procedure

In this section, we explain our aerosol sample collection process and show how we generated energy spectra using the IBA techniques.

3.1 Sample Collection

We collected aerosol samples at two sites in Schenectady, New York—the Vale Cemetery crematorium and the Union College Boathouse—in the summers of 2009 and 2010. The samples were collected using a nine stage cascade impactor [4] that separates particles according to their size. Particle diameters corresponding to >16, 16-8, 8-4, 4-2, 2-1, 1.0-0.5, 0.5-0.25, 0.25-0.12, and 0.12-0.06 μm were impacted on thin Kapton foils at each stage of the impactor, while a Nuclepore filter collected the remaining matter <0.06 μm in diameter. Our sampling apparatus is shown in Figure 2. A pump pulls air through the impactor which is designed to collect at a rate of 1 L/min. The flow rate is controlled and monitored with a valve and flow meter. The apparatus stood at each collection site for 2 days where we sampled approximately 3 m^3 of air.

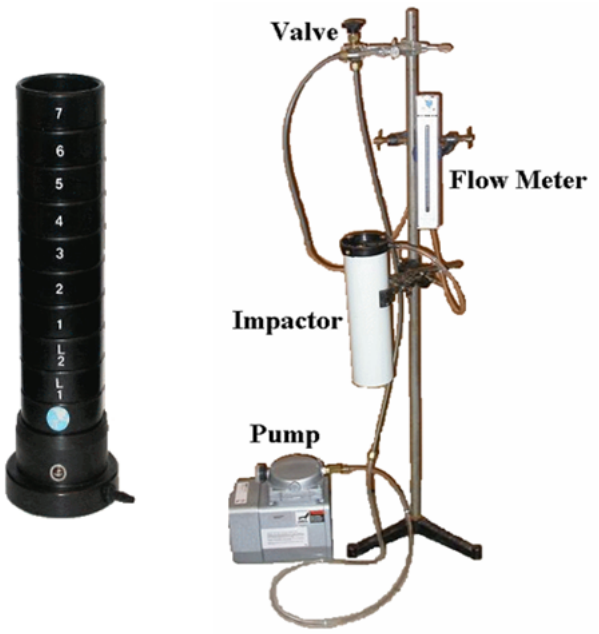

Figure 2: The nine stage impactor (left) and our sampling apparatus (right).

3.2 Scattering Experiments

The IBA experiments were performed at the Union College Ion-Beam Analysis Laboratory (UCIBAL). Since PIXE is our most used technique and most sensitive to protons [3], we used a proton beam to perform the scattering experiments. The protons were provided by a 1.1-MV Pelletron accelerator shown in Figure 3. They were produced in the source, then accelerated through the accelerator tank to energies up to 2.2 MeV. The quadrupole magnet focuses the beam, while the switcher magnet selects the correct beam energy by bending it 30° into the beam line to the scattering chamber.

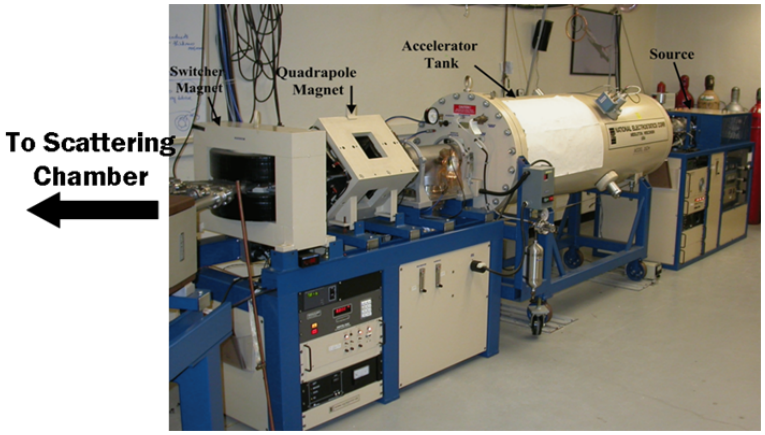

Figure 3: A photograph of Union College's 1.1-MV Pelletron accelerator showing the main components.

We probed our aerosol samples using proton beams with energies around 2 MeV and diameters of 2 mm. We measured beam currents between 2 and 4 nA in a Faraday cup positioned behind the scattering chambers, and determined the number of protons hitting the cup. The charge measured by the Faraday cup is approximately equal to the charge collected on a sample, which was typically 15 μC. In addition to examining aerosol samples, data were taken on a set of standards with each IBA technique.

The experimental apparatus for the PIXE measurements is shown in Figure 4.

The targets were set at the center of the scattering chamber at an angle of 45° to the beam to optimize the amount rays exiting the chamber through its thin beryllium vacuum window. The X-rays were detected with an Amptek silicon drift detector (SDD) [6] located 90° to the beam and 45° to the sample. The SDD detector was connected to a preamplifier which outputted to a PX4 digital pulse processor. This processor includes a multichannel analyzer which sorts pulses into each of its channels according to their amplitude. From the processor, signals proceeded to a computer where PIXE energy spectra were generated using the pulse heights with MCA8000A software [6]. We calibrated the PIXE detector with an americium-241 source.

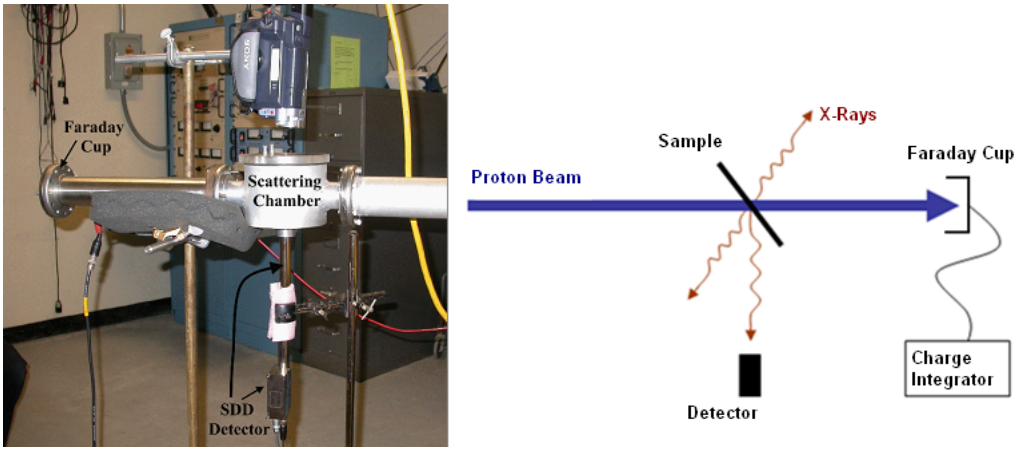

Figure 4: A picture and a schematic of the experimental apparatus for the PIXE measurements.

The experimental configuration for the PIGE measurements is shown in Figure 5. PIGE spectroscopy shared the same scattering chamber as PIXE, but used a germanium γ-ray detector to produce PIGE energy spectra. The signal from the γ-ray detector was processed with a preamplifier and a spectroscopic amplifier before it was digitized with an ORTEC TRUMP-PCI multichannel analyzer [5] and displayed on the computer with MAESTRO-32 software [5]. We calibrated this detector with the americium-241 source.

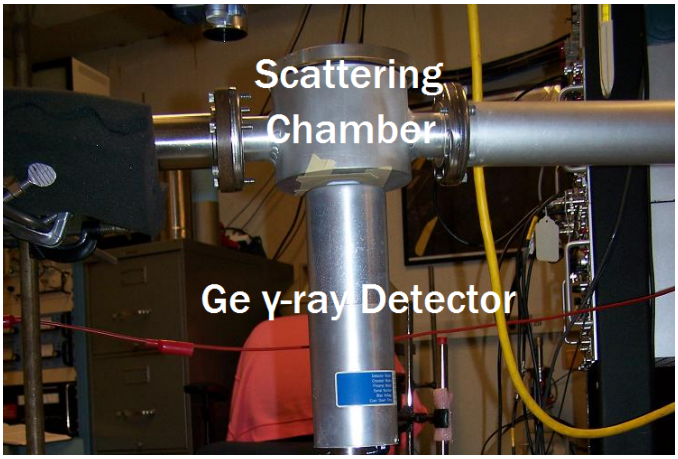

Figure 5: A picture of the experimental configuration for the PIGE measurements.

A photograph of the scattering chamber used in the RBS and PESA measurements is shown in Figure 6. The ion beam enters from the right and hits the target in the center. The vast majority of the ions pass through the target and are collected in the Faraday cup, but a small fraction are scattered to various angles. A silicon surface barrier detector was used to detect the ions at large angles for RBS and small angles for PESA. The signal provided by this charged particle detector was processed similarly to that of the PIGE detector, and we manipulated it to generate RBS and PESA energy spectra on the computer. This detector was also calibrated with the americium-241 source.

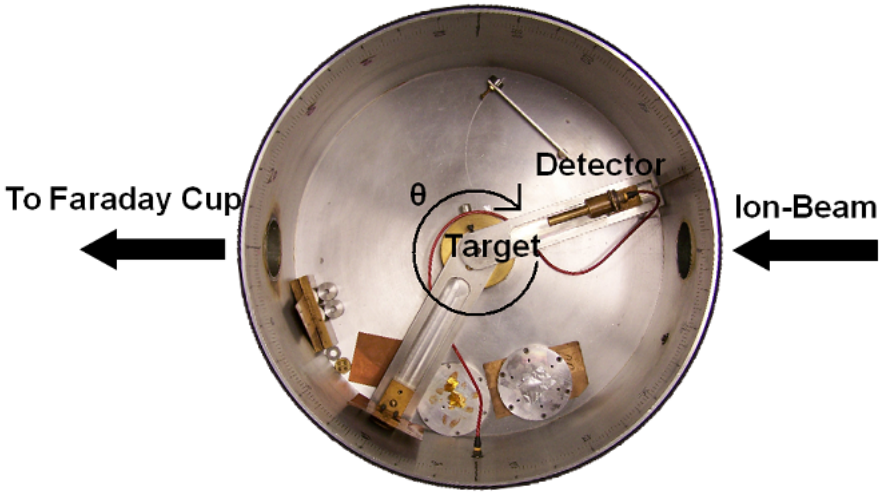

Figure 6: A photograph of the cluttered scattering chamber used in the RBS and PESA measurements. The target is positioned in the middle of the chamber and the silicon surface barrier detector can be moved to measure scattered ions at various angles.

4 Analysis

In this section, we discuss our analysis of the IBA energy spectra.

4.1 PIXE

A PIXE spectrum taken on an aerosol sample at the Union College Boathouse with particulate matter between 2 and 4 μm in size is shown in Figure 7. For comparison, also shown is a spectrum of a blank Kapton foil. A total charge of 15 μC was collected on each target. The peaks of the impacted foil spectrum are labeled, identifying most elements present in the aerosol sample.

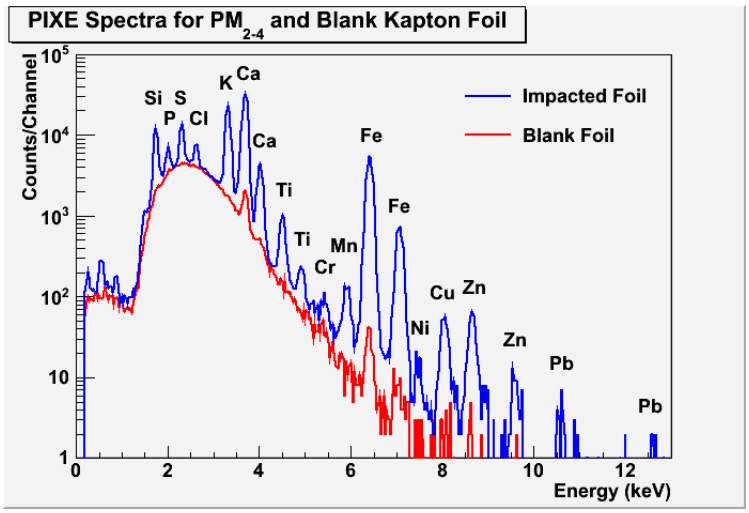

Figure 7: A comparison between PIXE spectra taken on an aerosol sample (blue) and a blank Kapton foil (red). The sample was for particulate matter between 2 and 4 μm.

The concentration C_z of an element Z in a sample is given by

$$C_z = \frac{Y_z}{Y_t \cdot H \cdot Q \cdot \varepsilon \cdot T} \tag{1}$$

where Y_Z is the intensity of the principle X-ray line for an element Z, Y_t is the theoretical intensity per micro-Coulomb of charge, H is the solid angle of the detector, Q is the measured beam charge incident on the sample, ε is the intrinsic efficiency of the detector, and T is the coefficient of transmission through any filters or absorbers between the target and the detector [1]. We used GUPIX software [7] to fit our PIXE spectra and extract C_z. A screen shot of a spectrum in GUPIX is shown in Figure 8.

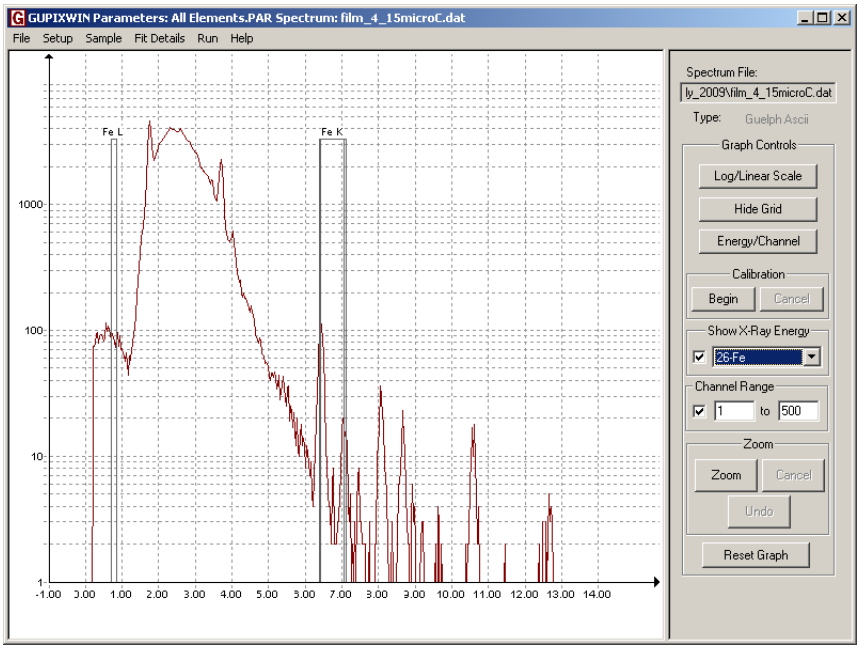

Figure 8: A PIXE spectrum in the GUPIX fitting software interface [7].

We provided GUPIX with input related to our experiment, such as beam type, beam energy, charge, and detector parameters. Then, the program used this input and the energy spectra to calculate elemental concentrations. GUPIX determined Y_Z by fitting the area under the peaks of the spectra, while Y_t, the theoretical cross sections of an element, is built into the program. Our SDD detector sat below a thin 76.2 μm beryllium window and 10 mm away from the targets, so GUPIX used this information to calculate the coefficient of transmission T. Lastly, we selected a detector type from a list stored in the program which gave a detector efficiency ε. Then, all the quantities required for GUPIX to compute C_z using Equation (1) were accounted for except H, the solid angle of the detector. Since we could not easily measure this value, we determined H using an experimental approach which involved taking data on a set of MicroMatter [8] standards with known concentrations. We ran 1 μC of charge on each of the sixteen standards, and Figure 9 shows a PIXE spectrum of an iron standard.

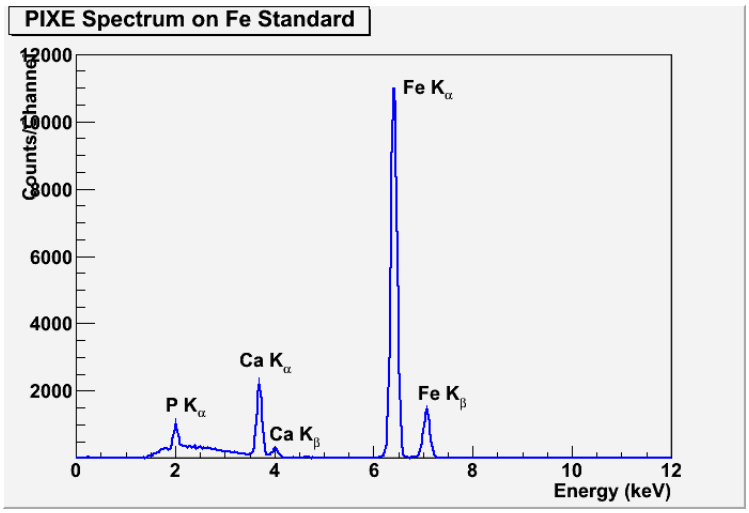

Figure 9: A PIXE spectrum taken on an iron standard for a total charge of 1 μC.

We took data on the standards with the H value set to 1 in GUPIX, and then compared each concentration to the known value provided by the MicroMatter [8] manufacturers. Thus, we extracted the H value by taking the ratio of the measured and known concentrations. Figure 10 shows the H value calculated for each standard. We averaged these values to obtain a final H value of 0.0023 ± 0.0002.

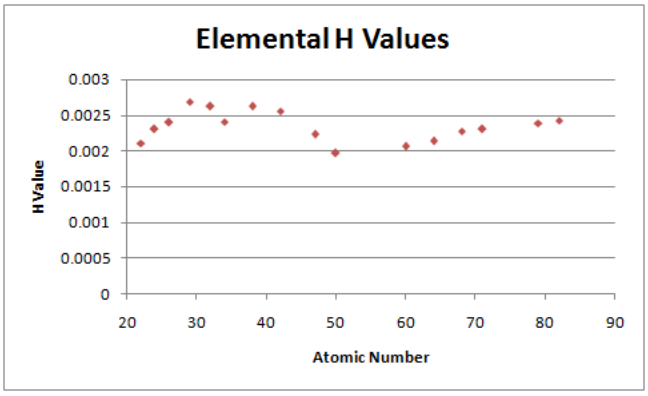

Figure 10: A comparison of the H values determined on a set of MicroMatter [8] standards.

Equipped with the H factor from Equation (1), we correctly fit our spectra with GUPIX and got elemental mass concentrations in mass per unit area. The fitted spectrum for the Boathouse aerosol sample with particulate matter between 2 and 4

μm is shown in Figure 11.

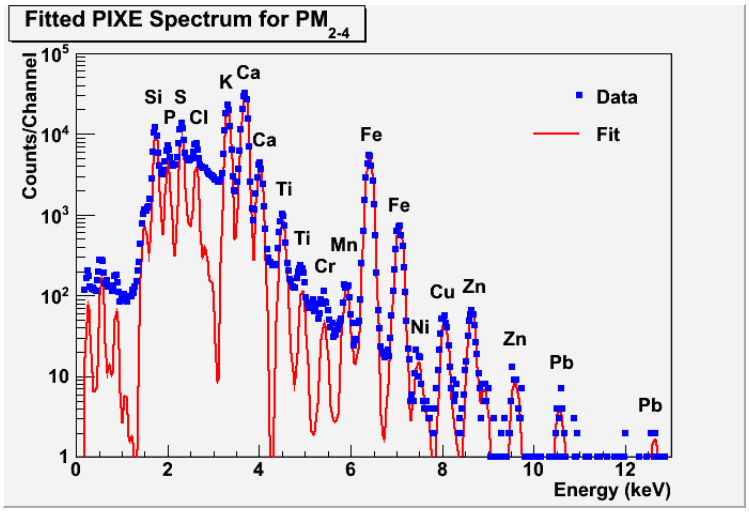

Figure 11: A PIXE spectrum taken on an aerosol sample with particulate matter in the 2 to 4 μm size range. The data are shown as blue points and the red curve is a fit to the data using GUPIX [7]. The fit to the background is not shown here.

Our determined concentrations are in mass per unit area C_A, and we must convert to concentration per unit volume C_V of sampled air to allow comparisons with other data. The conversion is

$$C_V = \left(\frac{P_{STP} \cdot T}{T_{STP} \cdot P}\right)\left(\frac{C_A \cdot A}{F \cdot t}\right) \tag{2}$$

where $T_{STP} = 25°C$ and $P_{STP} = 760\ Torr$ are the standard temperature and pressure, T and P are the average temperature and pressure during sample collection, A is the area of the sample collected on the Kapton film, F is the volumetric flow rate, and t is the collection time. At the Boathouse, we collected samples for 2 *days* at a flow rate of $1.0 \pm 0.1\ L/min$. The temperature and pressure, taken from the daily highs and lows of a nearby weather station, were $18.6 \pm 2.8\ °C$ and $753.0 \pm 3.2\ Torr$, respectively. Microscopic pictures of some samples taken at the Boathouse are seen in Figure 12, and the areas of these samples range from 0.105 ± 0.002 to $1.86 \pm 0.05\ mm^2$. The deposit corresponding to the spectrum in Figure 11 had an area of $1.86\ mm^2$ and sits in the upper right corner of the figure.

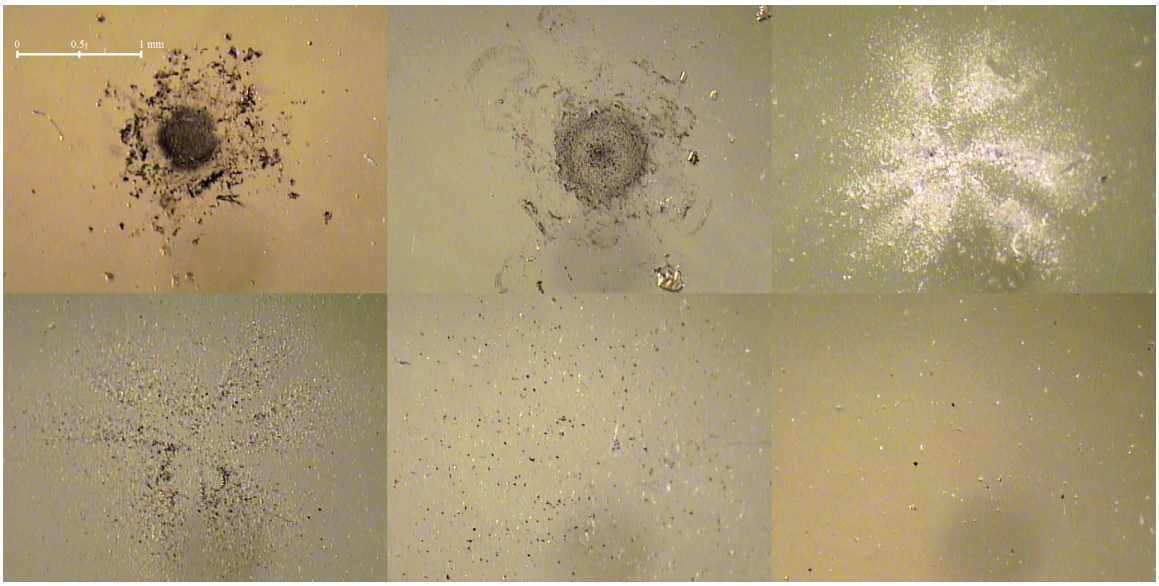

Figure 12: Pictures taken with a microscope of six samples impacted at the Boathouse (scale bar- 1 mm). The particle sizes in the samples from the top left in clockwise order range between 0.25-0.5, 0.5-1, 2-4, 4-8, 8-16, and >16 μm.

Table 1 shows the concentrations per unit area and per unit volume of the elements present in the aerosol sample with particulate matter between 2 and 4 μm collected at the Union College Boathouse. The error in C_A was determined by taking the square root of the sum of the squares of the statistical and fit error provided by GUPIX, while the error in C_V was calculated with the equation

$$\Delta C_V = C_V \sqrt{\left(\frac{\Delta C_A}{C_A}\right)^2 + \left(\frac{\Delta T}{T}\right)^2 + \left(\frac{\Delta P}{P}\right)^2 + \left(\frac{\Delta F}{F}\right)^2 + \left(\frac{\Delta A}{A}\right)^2} \tag{3}$$

where Δ represents the error in each quantity. Sources of error came from all the non-constant factors, but we did not consider error in the time, as it was too small to affect the calculations. Errors in the temperature and pressure were determined by taking the standard deviation of the data provided by the weather station. ΔF was provided by the manufacturer of the impactor [4]. We determined the error in the area of the sample deposits using ImageJ [9], an image processing program which returns selection areas, to analyze the microscopic pictures in Figure 12. For films

impacted with finer particles (Figure 12, top row), the deposits resemble a circular shape. So using ImageJ, we estimated each deposit area ten times with a circular selection, and took the average and standard deviation of the trials. We calculated areas of 0.537 ± 0.014, 0.585 ± 0.018, and 1.864 ± 0.053 mm^2 for the finer particles. The deposits corresponding to the coarser particles (Figure 12, bottom row) are more spread out than the finer deposits, and do not resemble a shape. But, these particles are larger and ImageJ was able to select the particles individually. We got areas of 0.824 ± 0.017, 0.357 ± 0.005, and 0.105 ± 0.002 mm^2 where ImageJ provided the error in the fits.

Table 1: The concentrations per unit volume (C_V) and per unit area (C_A) of elements present in an aerosol sample with particulate matter between 2 and 4 μm taken at the Union College Boathouse.

Element	C_A (ng/cm^2)	C_V (ng/m^3)
Si	2075 ± 57	10.9 ± 2.0
P	334 ± 16	1.76 ± 0.33
S	504 ± 12	2.65 ± 0.49
Cl	189.5 ± 6.6	1.00 ± 0.19
K	1075 ± 15	5.7 ± 1.0
Ca	1863 ± 23	9.8 ± 1.8
Ti	82.7 ± 2.8	0.43 ± 0.08
Cr	6.9 ± 1.6	0.04 ± 0.01
Mn	24.2 ± 2.2	0.13 ± 0.03
Fe	1525 ± 21	8.0 ± 1.5
Ni	6.9 ± 1.6	0.04 ± 0.01
Cu	34.9 ± 3.6	0.18 ± 0.04
Zn	55.9 ± 4.8	0.29 ± 0.06
Pb	30 ± 34	0.16 ± 0.18

4.2 RBS

An RBS spectrum taken at 160° on an aerosol sample at the Vale cemetery crematorium with particulate matter between 0.25 and 0.5 μm in size is shown in Figure 13. We probed this spectrum with a 1.8 MeV proton beam and a total charge of 15 μC was collected on the target.

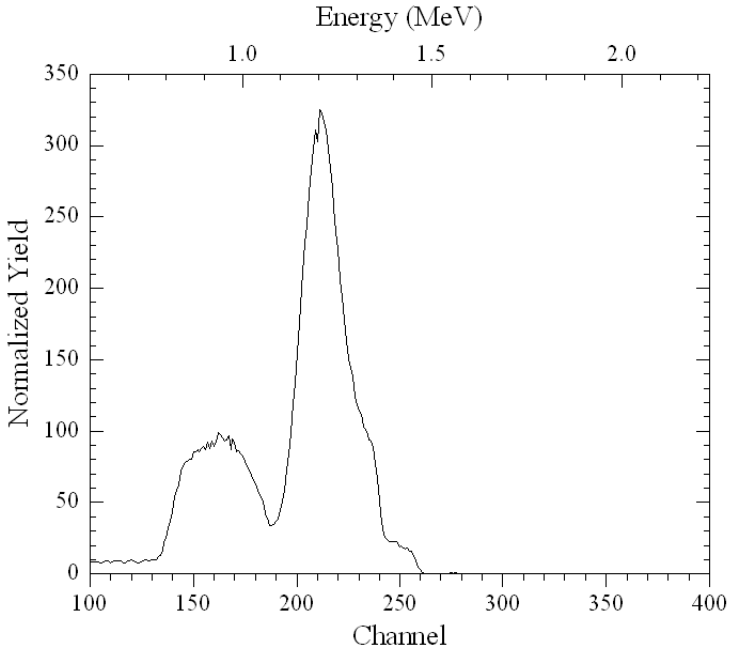

Figure 13: An RBS spectrum taken at 160° on an aerosol sample with particles between 0.25 and 0.5 μm from the Vale crematorium. We used a 1.8 MeV proton beam and collected 15 μC of charge on the sample.

Assuming an elastic collision between an incident ion and target, and applying conservation of momentum and kinetic energy, the mass M of the target nuclei is given by

$$M = m\left(\frac{\frac{K_f}{K_i} - 2\sqrt{\frac{K_f}{K_i}}\cos\theta + 1}{1 - \frac{K_f}{K_i}}\right) \tag{4}$$

where m is the mass of the scattered ion, K_i and K_f are the kinetic energies of the incident and scattered ions, and θ is the scattering angle. We used the Rutherford Universal Manipulation Program (RUMP) [10] to fit RBS energy spectra and extract elemental thicknesses.

We understand RUMP, as we successfully fit some RBS spectra with the program. Shown in Figure 14 is an RBS spectrum of a thin gold standard evaporated onto an aluminum backing taken at 140° using 3.3 MeV α-particles. We calibrated the energy spectrum in RUMP using the aluminum and carbon peaks in the spectrum. We extracted a gold thickness of about 26 Å which agreed well with the known value.

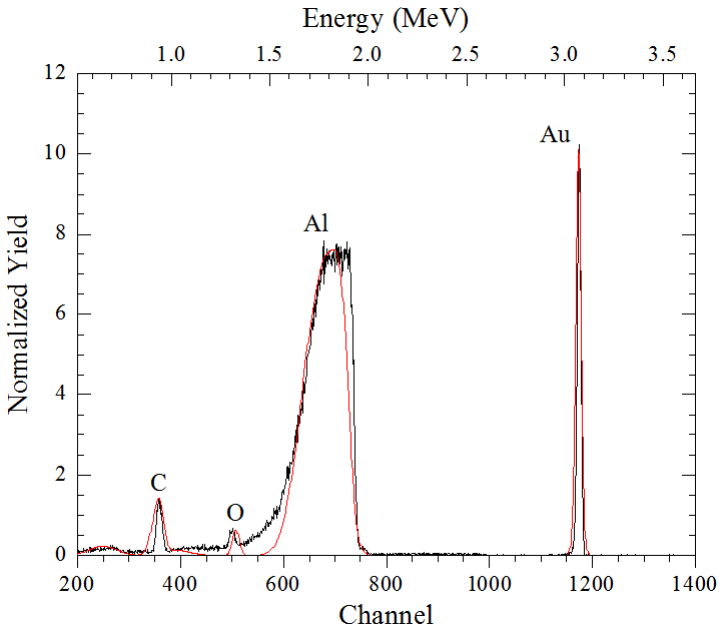

Figure 14: An RBS spectrum taken with a 3.3 MeV α-particle beam at 140° on an aluminum target with a thin layer of gold. The red curve is a fit to the data using RUMP [10].

A picture of the RUMP interface is shown in Figure 15. The commands pictured show the fitting process of the gold standard evaporated on an aluminum backing seen in Figure 14. We added varying amounts of gold, aluminum, carbon, and oxygen to the sample in different orders until RUMP produced a good fit. The main carbon and oxygen peaks in the figure represent the amount of these elements in front of the aluminum, while the neighboring smaller peaks represent the carbon and oxygen contaminants behind the aluminum.

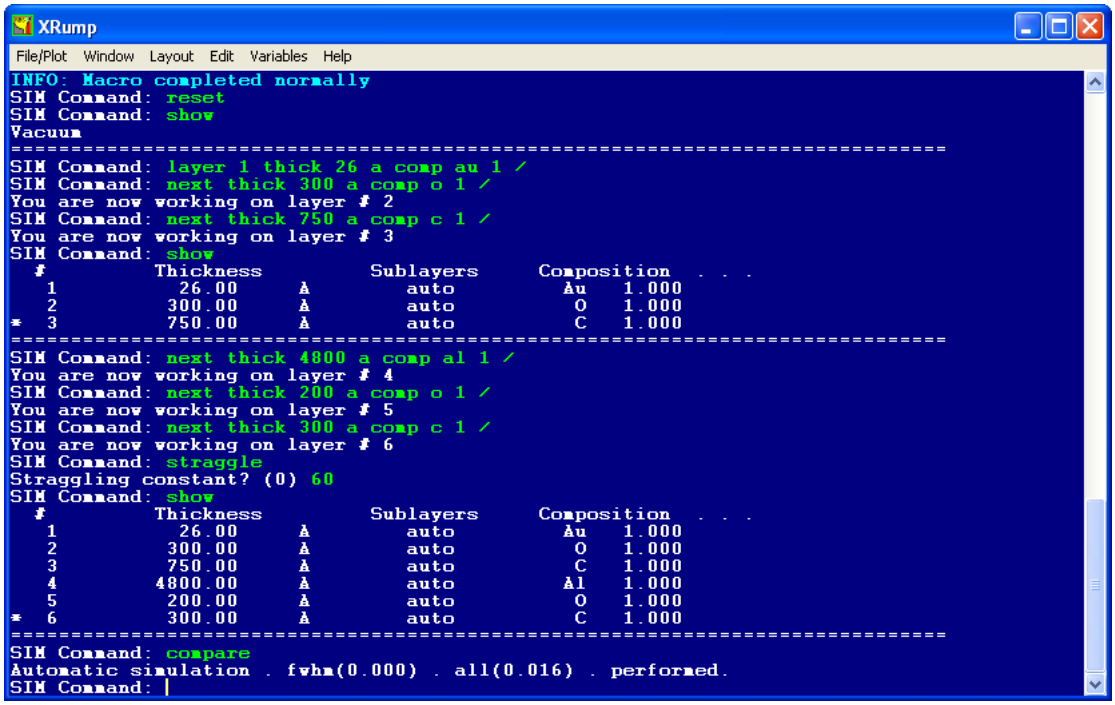

Figure 15: The RUMP program interface [10]. The commands pictured show the fitting process of the gold standard evaporated on an aluminum backing.

RBS analysis with α-particle beams is a commonly used technique in materials analysis and provides good mass resolution for a broad range of elements, but we are interested in making RBS measurements simultaneously with the other IBA techniques using proton beams. Unfortunately, by comparing Figure 13 and Figure 14, we observe the mass resolution using proton beams is not nearly as good as with α beams. So, we are currently working on fitting proton RBS spectra.

We took RBS spectra on gold, copper, and molybdenum standards evaporated on Mylar foils at angles of 140°, 150°, and 160° with a 1.8 MeV proton beam. Using these spectra, we calibrated RUMP. A graph of the RUMP proton calibration is shown in Figure 16. The line of best fit represents the channel number of the MCA converted to energy (keV) in RUMP, given by $Energy = (5.5 \pm 0.1) \cdot Channel + (27 \pm 34)$.

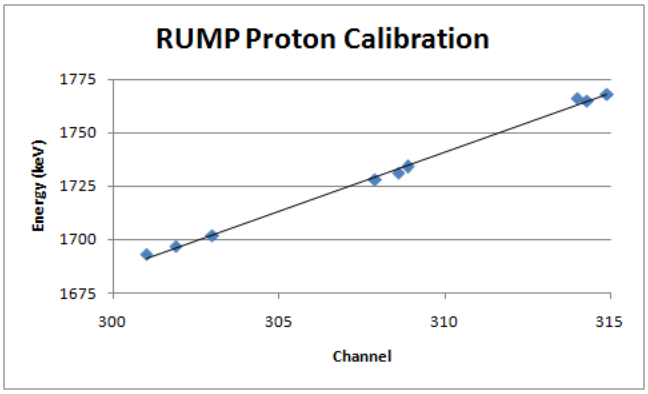

Figure 16: The RUMP energy calibration using the spectra of three standards taken at three different angles.

Figure 17 shows an RBS spectrum taken at 160° on a gold standard using a 1.8 MeV proton beam. The gold peak is fit well, but the Mylar peak is not. While our fit resembles the basic shape of the Mylar, it does not fill the peak completely. Similarly, we fit the copper and molybdenum peaks of the two other standards on Mylar backings, but in none of those were we able to fit the Mylar peak.

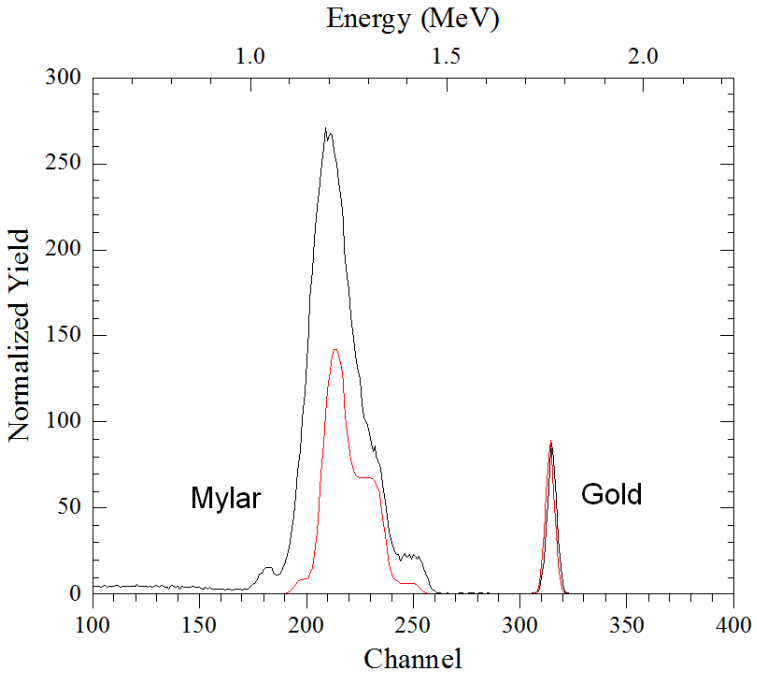

Figure 17: An attempt at fitting an RBS spectrum taken at 160° on a gold standard using a 1.8 MeV proton beam. A total charge of 10 μC was incident on the target.

We attempted to fit the RBS spectrum of the aerosol in Figure 13. This task proved more challenging than fitting a Mylar peak, and we were unsuccessful. More work needs to be done to understand how to fit these proton RBS spectra.

4.3 PIGE

A PIGE spectrum taken on a GdF_3 standard with a 1.8 MeV proton beam is shown in Figure 18. A total of 10 μC of charge was incident on the sample. We labeled most of the peaks according to Ref. [11]. We identified fluorine, magnesium, and aluminum in the spectrum—note that PIGE is not sensitive to gadolinium. Also, as is common in all PIGE spectra, we identified the electron-positron annihilation peak. When an electron and its antiparticle collide, they annihilate and yield two photons with energies equal to the rest energy of an electron or positron (511 keV). Using the GdF_3 PIGE spectrum, we can get information on fluorine, magnesium, and aluminum—all of which are light elements that the PIXE technique is less sensitive to.

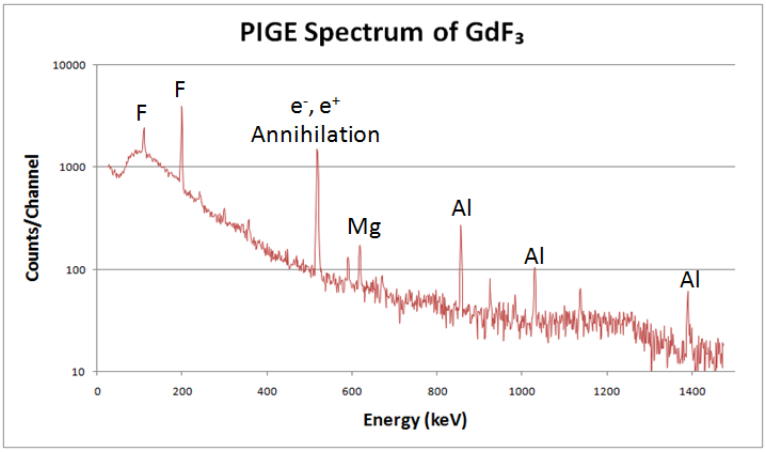

Figure 18: A PIGE spectrum taken on a GdF_3 standard with a 1.8 MeV proton beam. A total of 10 μC of charge was incident on the sample.

The formula for extracting elemental mass concentration is similar to the PIXE Equation (1). While PIXE and RBS have special fitting software, no such program

exists for PIGE. We may use a spectroscopy program like PeakFit [12] to fit PIGE spectra, and then use the elemental cross sections to complete the analysis. Figure 19 shows a PIGE spectrum of an aerosol sample with particulate matter between 0.25 and 0.5 μm taken at the Vale crematorium. We used a 1.8 MeV proton beam to obtain this spectrum and collected 10 μC of charge on the sample. From this spectrum, we could get information on the magnesium and aluminum present in the sample.

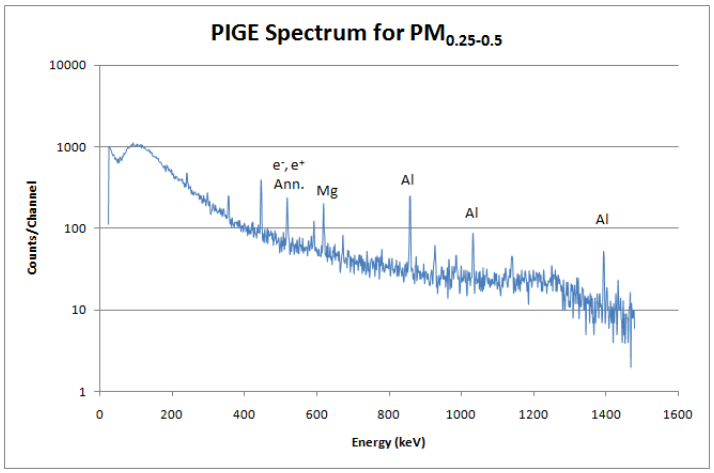

Figure 19: A PIGE spectrum taken on an aerosol with particles between 0.25 and 0.5 μm using a 1.8 MeV proton beam. A total of 10 μC of charge was incident on the sample.

4.4 PESA

Figure 20 shows a labeled PESA spectrum taken on a MoO_3 standard at a scattering angle of 40° using a 1.8 MeV proton beam. A total charge of 3 μC was incident on the target. We identified hydrogen and a combination of light elements, including carbon and oxygen, in the spectrum.

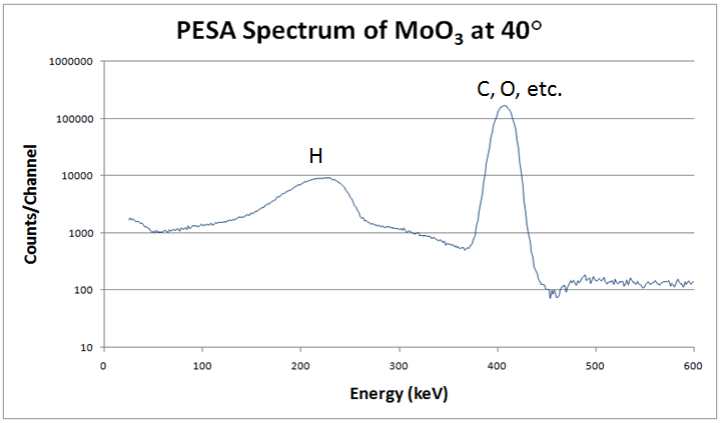

Figure 20: A PESA spectrum taken on a MoO_3 standard at a scattering angle of 40° using a 1.8 MeV proton beam. A total charge of 3 μC was incident on the target.

As with PIGE, there is no current fitting software programmed for PESA, and we may use PeakFit [12] to fit the peaks, and then apply the elemental cross sections to extract concentrations. Figure 21 shows a PESA spectrum taken on an aerosol sample with particulate matter between 0.25 and 0.5 μm at a scattering angle of 30° from the Vale crematorium. We used a 1.8 MeV proton beam and collected 3 μC of charge on the target. Once again, we identified hydrogen and other lighter elements in the spectrum.

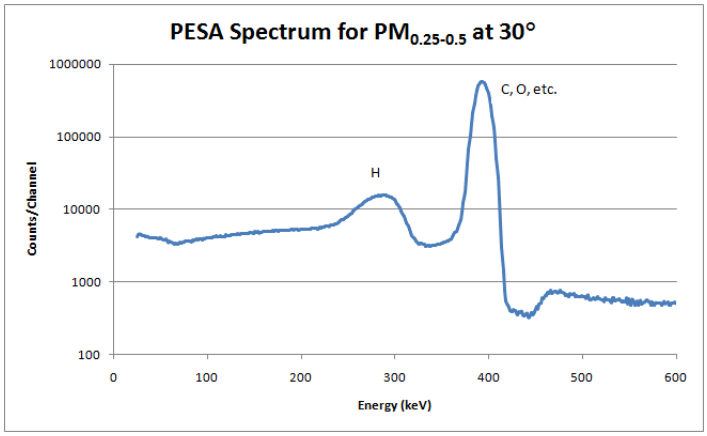

Figure 21: A PESA spectrum taken on an aerosol sample with particles between 0.25 and 0.5 μm at a scattering angle of 30° using a 1.8 MeV proton beam. A total charge of 3 μC was incident on the target.

5 Results

During the summers of 2009 and 2010, we sampled over 10 m^3 of air around Schenectady, NY. We successfully collected many aerosol samples and used four IBA techniques with the Union College particle accelerator to analyze the samples. Our main technique, PIXE is well understood and we used it to extract the concentrations of many elements in the samples, however, our complementary techniques are still very much in the development stage. In the RBS, PIGE, and PESA energy spectra, we were able to identify most of the peaks, but more progress needs to be made to fit the spectra and extract concentrations. Also, for aerosol samples analyzed with the RBS and PESA technique, we need to confirm that we are in fact hitting the target because some preliminary calculations have shown the difference between the spectra of the samples and the Kapton backing is minimal. Here, we present the results of our IBA analysis.

5.1 PIXE

We successfully developed a method for fitting PIXE energy spectra and extracting elemental concentrations using GUPIX [7]. Data from the PIXE Union College boathouse run from the summer of 2009 are shown in Figure 22 and Tables 2 and 3.

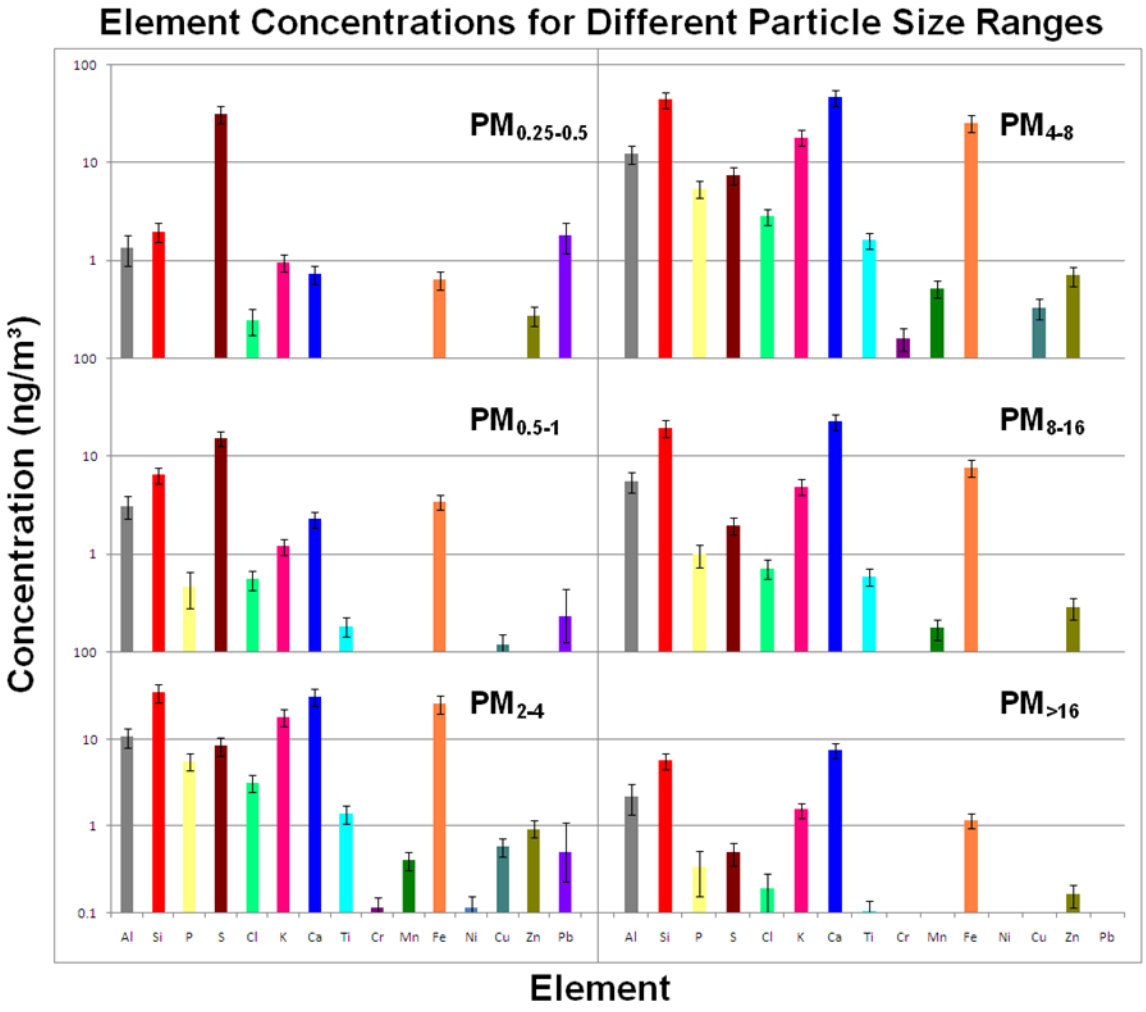

Figure 22: A bar graph of the elemental concentrations extracted from the summer 2009 Union College boathouse run using PIXE analysis. The aerosol samples contain particle sizes ranging from 0.25-0.5 μm to $>$16 μm.

Table 2: A table of the elemental concentrations extracted from the summer 2009 Union College boathouse run using PIXE analysis. The aerosol samples contain particle sizes ranging from 0.25-0.5 μm to 2-4 μm.

Element	$PM_{0.25-0.5}$ (ng/m^3)	$PM_{0.5-1}$ (ng/m^3)	PM_{2-4} (ng/m^3)
Al	0.24 ± 0.08	0.38 ± 0.10	3.36 ± 0.70
Si	0.35 ± 0.07	0.79 ± 0.15	10.9 ± 2.0
P	0	0.06 ± 0.02	1.76 ± 0.33
S	5.6 ± 1.0	1.85 ± 0.34	2.65 ± 0.49
Cl	0.04 ± 0.01	0.07 ± 0.06	1.0 ± 0.2
Ar	0.001 ± 0.006	0.009 ± 0.007	0.03 ± 0.02
K	0.17 ± 0.03	0.15 ± 0.03	5.7 ± 1.0
Ca	0.13 ± 0.02	0.28 ± 0.05	9.8 ± 1.8
Ti	0.005 ± 0.002	0.022 ± 0.005	0.44 ± 0.08
Cr	0.004 ± 0.002	0.007 ± 0.002	0.04 ± 0.01
Mn	0.002 ± 0.002	0.010 ± 0.003	0.13 ± 0.03
Fe	0.11 ± 0.02	0.42 ± 0.08	8.0 ± 1.5
Ni	0.003 ± 0.002	0.001 ± 0.002	0.04 ± 0.01
Cu	0.013 ± 0.004	0.014 ± 0.004	0.18 ± 0.04
Zn	0.05 ± 0.01	0.010 ± 0.004	0.29 ± 0.06
Se	0.010 ± 0.007	0.009 ± 0.007	0
Br	0.02 ± 0.01	0.011 ± 0.009	0.02 ± 0.02
Pb	0.32 ± 0.11	0.03 ± 0.05	0.16 ± 0.18

Table 3: A table of the elemental concentrations extracted from the summer 2009 Union College boathouse run using PIXE analysis. The aerosol samples contain particle sizes ranging from 4-8 μm to >16 μm.

Element	PM_{4-8} (ng/m^3)	PM_{8-16} (ng/m^3)	$PM_{>16}$ (ng/m^3)
Al	1.67 ± 0.34	0.32 ± 0.08	0.04 ± 0.02
Si	6.0 ± 1.1	1.14 ± 0.21	0.10 ± 0.02
P	0.73 ± 0.14	0.06 ± 0.02	0.006 ± 0.003
S	1.00 ± 0.18	0.12 ± 0.02	0.008 ± 0.002
Cl	0.38 ± 0.07	0.042 ± 0.009	0.003 ± 0.002
Ar	0.01 ± 0.01	0.005 ± 0.004	0
K	2.44 ± 0.44	0.29 ± 0.05	0.027 ± 0.005
Ca	6.2 ± 1.1	1.31 ± 0.24	0.13 ± 0.02
Ti	0.22 ± 0.04	0.034 ± 0.007	0.002 ± 0.001
Cr	0.022 ± 0.005	0.004 ± 0.002	0
Mn	0.07 ± 0.01	0.010 ± 0.002	0
Fe	3.42 ± 0.62	0.45 ± 0.08	0.020 ± 0.004
Ni	0.004 ± 0.003	0.001 ± 0.001	0
Cu	0.04 ± 0.01	0.004 ± 0.002	0
Zn	0.09 ± 0.02	0.017 ± 0.004	0.003 ± 0.001
Se	0	0	0
Br	0	0	0
Pb	0	0	0

With the elemental concentrations across six different particle sizes, we can make some preliminary remarks about the data. There are considerable concentrations of sulfur in the aerosol samples, particularly for small particles. Sulfur is a main component of acid rain and understanding the dependence of the concentration on aerosol particle size is important for addressing the acid rain problem in upstate New York, particularly in the Adirondack Mountains. Industrious regions throughout Ohio, Illinois, Indiana and Pennsylvania are main contributors of the sources of acid rain—sulfur dioxide and nitrogen oxides—present in Adirondack air [13]. Studies show a dangerous increase in the acidification of lakes, streams, and soil in the mountainous region, which has a damaging effect on vegetation and wildlife [14].

Also, there are measurable concentrations of lead in the small particle aerosols. This observation certainly warrants further study because the toxicity of lead is well

known and airborne contaminants with diameters less than 2.5 μm present special health risks. In 2008, the U.S. Environmental Protection Agency lowered the legal limit for the safe amount of lead present in air to 150 ng/m^3 [15]. Our results show the amount of lead present at the boathouse is well below this limit.

Due to their potentially dangerous health effects, we will continue to monitor sulfur and lead at other sampling locations.

5.2 Complementary Techniques

We successfully used RBS, PIGE, and PESA techniques at the UCIBAL to generate energy spectra of standards and aerosol samples.

For RBS, we understand the fitting software RUMP [10], as we were able to fit a spectrum taken on a gold standard with α particles. But, RBS analysis using a proton beam is more difficult and requires more work. Then, once we learn to fit RBS proton spectra, more work is necessary to extract mass concentrations.

With PIGE, we identified most of the peaks in the standard and aerosol sample spectra from a list of fluorine, magnesium, and aluminum transitions. We must expand our list of elemental transitions to label all the peaks in the spectra. Though we have only identified these three elements in our PIGE spectra, our research program would still benefit from this small PIGE contribution, as the PIXE limits of detection for these elements is not good. After identifying more peaks, we need to fit the PIGE spectra and work to extract elemental concentrations.

The PESA spectra have two main peaks. We do not fully understand what elements contribute to the non-hydrogen peak. However, this is not crucial because we are mainly interested in analyzing the hydrogen peak, as the other IBA techniques do not reveal information on hydrogen so accurately. Once we fit this peak, we must work to extract a hydrogen concentration.

6 Conclusion

We reported on the progress made in developing the IBA techniques of PIXE, RBS, PIGE, and PESA in the analysis of atmospheric aerosols at the UCIBAL. We successfully created a system for collecting air samples and generating energy spectra with the techniques using the particle accelerator. We fully developed the PIXE technique, and presented complete data from an aerosol run at the Union College boathouse. Though this IBA technique is the main focus of our project, it lacks analysis of lighter elements, and so we need the other techniques to analyze these lighter elements, and complement PIXE. We are still developing the RBS, PIGE, and PESA techniques, and in the future, we aim to have as much confidence in these results as we do with PIXE.

Then, once we have fully developed these complementary techniques, we will expand our sampling from aerosols to water, tree, or soil collection. In the manner of Ref. [3], we will identify the transformation and transport of pollution around New York by estimating the sources of the pollution. The sources will vary in differing amounts from region to region. For example, we will use our measured elemental concentrations in different types of samples to estimate the amount of black carbon (incomplete combustion of fossil fuels, biofuel, and biomass), ammonium sulfate (commercial salt), sea salt, or soil spray in one area of New York compared to another area. This way, the results are more useful and easier to interpret, as opposed to simply reporting bare elemental concentrations. Finally, with all of this data, we will form conclusions on the state of pollution in New York, and provide information that can be used to aid in its removal.

References

[1] S.A.E. Johansson, J.L. Campbell, and K.G. Malmqvist, "Particle-Induced X-Ray Emission Spectrometry (PIXE)" (Wiley, New York, 1995).

[2] Proton Induced X-ray Emission (PIXE) - EAI - Elemental Analysis, Inc., http://www.elementalanalysis.com/.

[3] D.D. Cohen et al., "IBA methods for characterization of fine particulate atmospheric pollution: a local, regional and global research problem," Nuclear Instruments and Methods B 219-220, 145 (2004); and references therein.

[4] PIXE International Corporation, P.O. Box 2744, Tallahassee, FL 32316 USA, http://pixeintl.com/.

[5] Multichannel Analyzers | ORTEC Scientific Equipment, http://www.ortec-online.com/Solutions/multichannel-analyzers.aspx.

[6] X-Ray detectors, Gamma Ray detectors, Charge Sensitive Preamplifiers, http://www.amptek.com/.

[7] GUPIX, the versatile PIXE spectrum fitting software, University of Guelph, http://pixe.physics.uoguelph.ca/gupix/main/.

[8] MicroMatter Co., 18218 18th Ave. NW, Arlington, WA 98223, USA.

[9] ImageJ, http://rsbweb.nih.gov/ij/.

[10] GENPLOT and RUMP Documentation, http://genplot.com/.

[11] C. Boni *et al.*, "Prompt Gamma Emission Excitation Functions for PIGE Analysis of Li, B, F, Mg, Al, Si, and P in Thin Samples," Nuclear Instruments and Methods B **35**, 80-88 (1988).

[12] PeakFit - The Automatic Choice for Spectroscopy, Chromatography and Electrophoresis, http://www.sigmaplot.com/products/peakfit/peakfit.php.

[13] J. Jenkins, K. Roy, C. Driscoll, and C. Buerkett, "Acid Rain and the Adirondacks: A Research Summary," Adirondack Lakes Survey Corporation, 1115 NYS Rt.86, P.O. BOX 296, Ray Brook, NY 12977 (2005).

[14] G.B. Lawrence et al., J. Environ. Qual. 37 (6), 2264 (2008).

[15] Lead Air Quality Standards | Lead | US EPA, http://www.epa.gov/oaqps001/lead/standards.html.